ChemPubSoc Europe

DOI: 10.1002/cctc.201402146

Insight into the Formation and Reactivity of Framework-Bound Methoxide Species in H-ZSM-5 from Static and Dynamic Molecular Simulations

Jeroen Van der Mynsbrugge, Samuel L. C. Moors, Kristof De Wispelaere, and Veronique Van Speybroeck*[a]

Framework-bound methoxides occur as intermediates in the stepwise mechanism for zeolite-catalyzed methylation reactions. Herein, the formation of methoxides from methanol or dimethyl ether in H-ZSM-5 is investigated by a combination of static and dynamic simulations, with particular focus on the effect of additional water and methanol molecules on the mechanism and kinetics. Metadynamics simulations allow partitioning the reaction path into distinct phases. Proton transfer from the zeolite to the reactants is found to be the rate-limiting phase in the methoxide formation. Additional methanol molecules only assist the proton transfer in the methoxide formation from methanol, whereas the reaction from dimethyl ether does not benefit from methanol assistance. Once formed, methoxides are found to be as reactive toward alkene methylation as methanol and dimethyl ether.

Introduction

Methylation reactions catalyzed by Brønsted acid zeolites are essential to many industrially important processes, for example, the conversion of methanol to commodity chemicals such as polymer-grade ethene and propene in the methanol-to-olefins process (MTO).[1] Methylations of aromatic and aliphatic compounds are crucial in all MTO mechanisms proposed to date: these reactions are the premier way of incorporating methanol into the hydrocarbon pool present inside the catalyst pores, from which olefins are ultimately eliminated.[2,3] Additionally, methylation of alkenes or arenes is one of the few reactions that are amenable to direct kinetic measurements. For these reasons, methylation reactions have been the subject of numerous experimental and theoretical studies.[4–11] Svelle et al. have recently compiled a review of the literature on this topic.[12] In spite of ample research dedicated to this reaction, the question remains whether the prevailing mechanism is direct (concerted) or rather indirect (stepwise). In the concerted mechanism, methylation occurs in a single step, with physisorbed methanol or dimethyl ether acting as the methylating agent. In the stepwise mechanism, framework-bound methoxide species are formed prior to the actual methylation.[10–12]

Spectroscopic studies using both FTIR[13–15] and magic-angle spinning ^{13}C NMR[16–19] techniques have demonstrated the existence of methoxide species, and methoxides have also been proven active as a methylating agent.[13,14,16,17,19–21] However, these findings relate to a sequential approach: methoxides are formed when methanol is fed to the zeolite at a modest temperature (150 °C), whereas methylation occurs when alkenes or arenes are added and the temperature is raised to 220–260 °C. In a recent study, Saepurahman et al. performed in situ FTIR measurements during benzene methylation by methanol on H-ZSM-5 and H-beta, and reported that no methoxide species associated with Brønsted acid sites were observed during steady-state co-reaction.[6]

From these spectroscopic studies, it is thus unclear in how far methoxides are formed during steady-state operation, or which methylation mechanism prevails at the various stages of the process. Theoretical modeling of individual reaction steps has proven to be invaluable to attain a more profound understanding of experimental data. However, among the plethora of theoretical papers on the MTO process and methylation reactions in particular, only a few compare the direct and indirect mechanism.[22,23] In an early study, Vos et al. found that the barrier for methoxide formation is higher than that for the ensuing methylation step.[22] This finding implies that, if methylation occurred through an indirect mechanism, the methoxide formation would be the rate-determining step, and the overall methylation rate would be independent of the alkene or arene, which is in contradiction to kinetic measurements. As it provides good agreement with experimental kinetic data, subsequent theoretical studies employing increasingly sophisticated methods have largely focused on the concerted mechanism without intermediates, whereas the methoxide formation has not been explored in great detail.

In most theoretical studies, the methoxide formation was modeled in its simplest form: a single molecule of methanol or dimethyl ether is protonated by a Brønsted acid site, and a methyl group is transferred to a framework oxygen, releasing

[a] Dr. J. Van der Mynsbrugge, Dr. S. L. C. Moors, K. De Wispelaere, Prof. Dr. V. Van Speybroeck
Center for Molecular Modeling
Ghent University
Technologiepark 903, 9052 Zwijnaarde (Belgium)
E-mail: veronique.vanspeybroeck@ugent.be

Supporting information for this article is available on the WWW under http://dx.doi.org/10.1002/cctc.201402146.

a water or methanol molecule (Scheme 1 a). However, industrial methanol conversion processes typically operate at high methanol partial pressures to maximize the overall efficiency. Water is often present in the feed, and sometimes added in the form of process condensate or steam to tune the product selectivity. Additionally, dehydration of methanol to dimethyl ether is known to be fast compared to methylation. Under these conditions, a mixture of methanol, dimethyl ether, and water molecules are likely to be present in the vicinity of a given active site. In a paper by Lesthaeghe et al., participation of an additional water or methanol molecule in the methoxide formation (Scheme 1 b) was found to stabilize the transition state, resulting in a significantly lower reaction barrier.[24]

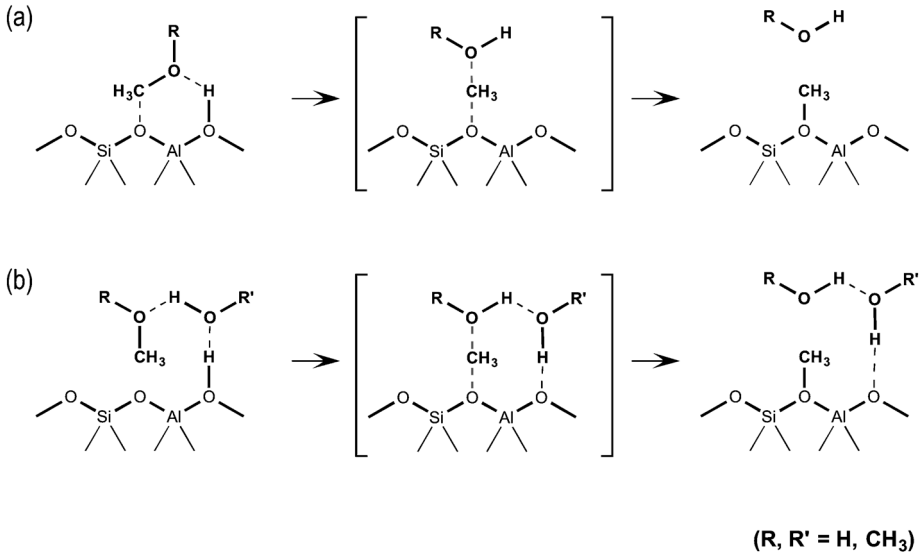

Scheme 1. a) Unassisted and b) assisted methoxide formation.

Finally, limited computational resources at the time of publication of the papers by Vos et al. and Lesthaeghe et al. imposed the use of fairly small cluster models representing only the Brønsted acid functionality of the zeolite. In reality, the zeolite framework also provides long-range stabilizing effects on the various intermediates formed during reaction. More recently, Maihom et al. modeled the methoxide formation in H-ZSM-5 using the ONIOM approach on a large cluster model to account for the zeolite framework.[23] Although this constitutes a significant improvement over earlier studies, only electronic barriers were reported. Given the high temperatures at which methanol conversion processes typically take place, entropic contributions are essential to the discussion.

From a modeling point of view, accounting for additional molecules is quite challenging. Routinely used static methods that take only one point of the potential energy surface into account may provide some valuable insights, but because the position of the additional participating molecules is not uniquely defined, several local minima exist on the potential energy surface, and it is virtually impossible to single out one minimum that represents all relevant aspects of the reaction mechanism. This was recently highlighted in a study on the methylation of benzene, in which the effect of additional methanol molecules was investigated using molecular dynamics simulations.[25] Apart from the typical direct methylation route occurring at the acid site of the zeolite, the formation of methanol clusters was observed, which was found to affect the reaction mechanism and methylation rate.[25]

Herein, we present an in-depth study on the formation of methoxide species and their reactivity toward methylation of alkenes. All reactions are modeled in H-ZSM-5, because most of the previously reported data is available for this catalyst. The topology of the zeolite is taken into account and the role of additional methanol and water on the methoxide formation is investigated. Static calculations are supplemented by molecular dynamics simulations to attain a more complete sampling of the free-energy surface and a better description of the various configurations of the guest molecules and the flexibility the zeolite framework at typical operating temperatures. For the simulation of reactions, which are rare events during a standard molecular dynamics simulation, the metadynamics approach is used to obtain efficient sampling of otherwise inaccessible regions of the free-energy surface.[26–28]

Zeolite models

A model for the H-ZSM-5 catalyst is constructed by inserting a substitutional aluminum defect at the T12 position of an MFI unit cell, and a charge-compensating proton on an adjacent oxygen accessible from the straight and sinusoidal channels (O20, O24, or O11; see Figure 1). The Al defect gives rise to a Brønsted acid site situated at the channel intersection. Although Sklenak and co-workers have shown that the actual Al distribution in MFI materials is kinetically controlled during the zeolite synthesis,[29–31] this location is often selected in theoretical studies, because it can also accommodate bulkier molecules. The salient topological features of the zeolite framework are taken into account in both the static and dynamic simulations. In the static calculations, the catalyst is represented by a large cluster of 46 T atoms (Figure 1), which is selected to provide an accurate description of the active site and its surroundings. Geometry optimizations and frequency calculations are performed by using the two-level ONIOM(B3LYP/6-31+G(d,p):MNDO) method, and the energies of the various stationary points are refined by single-point calculations at the ωB97X-D/6-31+G(d,p) level of theory. Ab initio molecular dynamics (MD) and metadynamics simulations were performed on the complete unit cell using periodic boundary conditions.

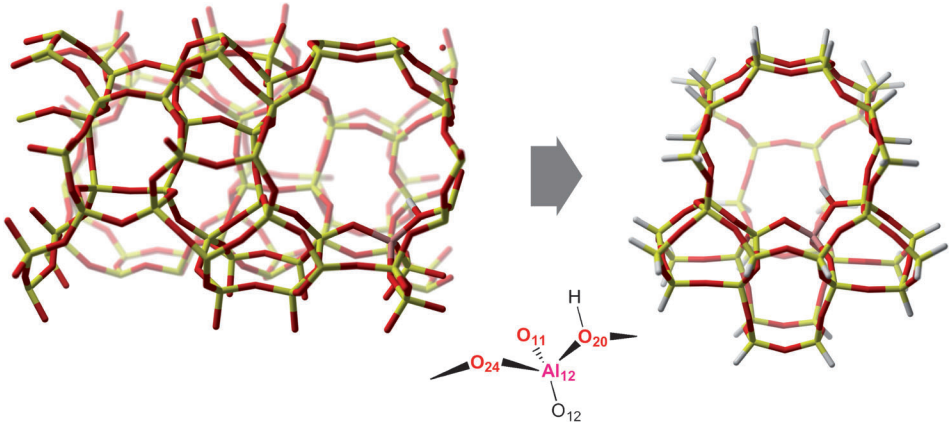

Figure 1. Models for H-ZSM-5: (left) complete unit cell: Al in the T12 position; charge-compensating proton on adjacent oxygen accessible from the channels (O20, O24, or O11); (right) finite cluster model (46 T atoms). Color code: Si, yellow; Al, pink; O, red; H, white.

MD simulations were performed in the NVT ensemble at 670 K using the revPBE−D3 functional with the DZVP-GTH basis set. Additional details are given in Experimental Section.

Results and Discussion

The formation of framework-bound methoxide groups from methanol and dimethyl ether as methyl source was investigated, both by a monomolecular mechanism and in the presence of additional protic molecules. Any zeolite-catalyzed reaction can be thought of as a two-step process (Scheme 2): reactants

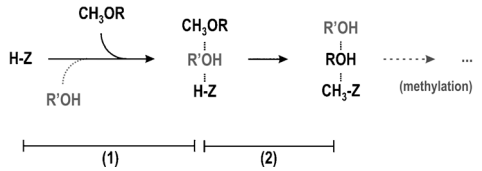

Scheme 2. Methoxide formation as a two-step process: (1) reactants adsorb at the active site; (2) preactivated complex is reorganized. (R, R′ = H, CH_3).

gather at an active site to form a preactivated complex (1), which is subsequently reorganized in the actual reaction step (2). In the following, both the adsorption and the methoxide formation are discussed by using a combination of static and dynamic molecular modeling methods. Finally, the methylation of ethene, propene, and *trans*-2-butene with framework-bound methoxides is compared to the concerted methylation with hydrogen-bonded methanol and dimethyl ether.

Adsorption of reactants at the Brønsted acid sites

Adsorption of a single methanol, dimethyl ether, or water molecule

The most stable configurations for the adsorption of a single methanol, water, or dimethyl ether molecule at a Brønsted site are represented in Figure 2. Adsorption enthalpies, entropies, and free energies at 623 K are summarized in Table 1. Methanol and water both form a strong hydrogen bond with the Brønsted acid site, and a weaker one with the neighboring framework oxygen (Figure 2a, b.). The adsorption enthalpies (ΔH_{ads}) for methanol and water (−105 kJ mol^{-1} and −83 kJ mol^{-1}, respectively) correspond fairly well with the experimental heats of adsorption at 400 K reported by Lee et al (−115 ± 5 kJ mol^{-1} and −90 ± 10 kJ mol^{-1}, respectively).[32] Dimethyl ether can form only one hydrogen bond with the zeolite framework (Figure 2c), but is still found to adsorb more strongly (ΔH_{ads} = −116 kJ mol^{-1}). The difference in adsorption enthalpy between methanol and dimethyl ether of 11 kJ mol^{-1} is in line with the additional heat of adsorption of 10-15 kJ mol^{-1} per carbon atom reported in previous experimental and theoretical adsorption studies on homologous series of alkanes, alkenes, alcohols, and nitriles.[32–38] The formation of hydrogen bonds restricts conformational freedom in the adsorption complexes. Hence, a greater entropy loss is incurred upon adsorption of methanol (ΔS_{ads} = −150 J mol^{-1} K) than of dimethyl ether (ΔS_{ads} = −139 J mol^{-1} K^{-1}), resulting in free energies of adsorption (ΔG_{ads}) at 623 K of −11 kJ mol^{-1} for methanol and −29 kJ mol^{-1} for dimethyl ether. The entropy loss for water is the same as for dimethyl ether (ΔS_{ads} = −139 J mol^{-1} K^{-1}), resulting in a positive adsorption free energy (ΔG_{ads} = + 4 kJ mol^{-1}).

Co-adsorption of methanol or dimethyl ether on water or methanol

An isolated methanol or water molecule can form two hydrogen bonds upon adsorption at a Brønsted acid site, with a lattice oxygen acting as the acceptor of the second, weaker hydrogen bond (see below). If additional adsorbate molecules are present, these can act as hydrogen bond acceptor instead, forming a complex. In this section, we consider the formation of such complexes, specifically focusing on the cases in which a methanol or dimethyl ether molecule adsorbs onto a previously adsorbed water or methanol molecule (Figure 3). From these complexes, methoxide formation may also proceed; the reaction is then assisted by the first adsorbate, acting as a proton shuttle between the zeolite Brønsted acid site and the reacting methanol or dimethyl ether (see Scheme 1).

Adsorption enthalpies, entropies, and free energies associated with the complexes are also included in Table 1. In all four cases, co-adsorption of the second molecule results in an increased adsorption enthalpy, but is also accompanied by an increased entropy loss. At 623 K, the entropic penalty cancels out the enthalpic stabilization for co-adsorption of methanol

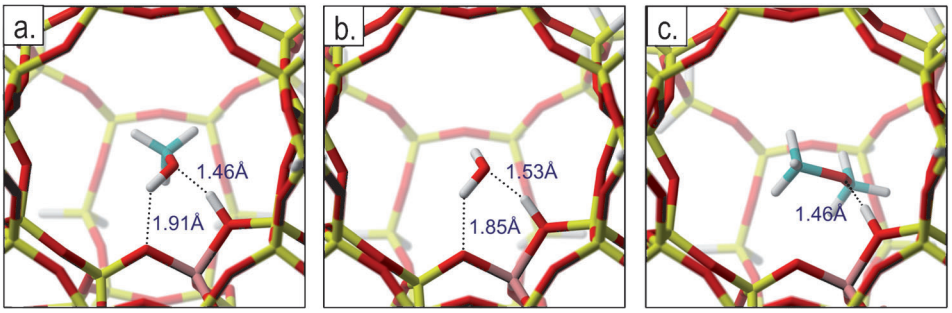

Figure 2. Adsorption of a) methanol, b) water, and c) dimethyl ether at a Brønsted site in H-ZSM-5. Color code: Si, yellow; Al, pink; O, red; H, white; C, light blue.

Table 1. Adsorption and co-adsorption of methanol, water, and dimethyl ether at a Brønsted acid site in H-ZSM-5. Adsorption enthalpies (ΔH_{ads}), entropies (ΔS_{ads}), and free energies (ΔG_{ads}) reported at 623 K. Level of theory electronic energy: ωB97X-D/6-31 g(d,p)//ONIOM(B3LYP/6-31 g(d,p):MNDO).

	ΔH_{ads} [kJ mol^{-1}]	ΔS_{ads} [J mol^{-1} K^{-1}]	$-T\Delta S_{ads}$ [kJ mol^{-1}]	ΔG_{ads} [kJ mol^{-1}]
MeOH	−105	−150	94	−11
H_2O	−83	−139	87	4
DME	−116	−139	87	−29
H_2O + MeOH	−166	−284	177	11
MeOH + MeOH	−172	−284	177	4
H_2O + DME	−154	−273	170	17
MeOH + DME	−173	−280	175	1

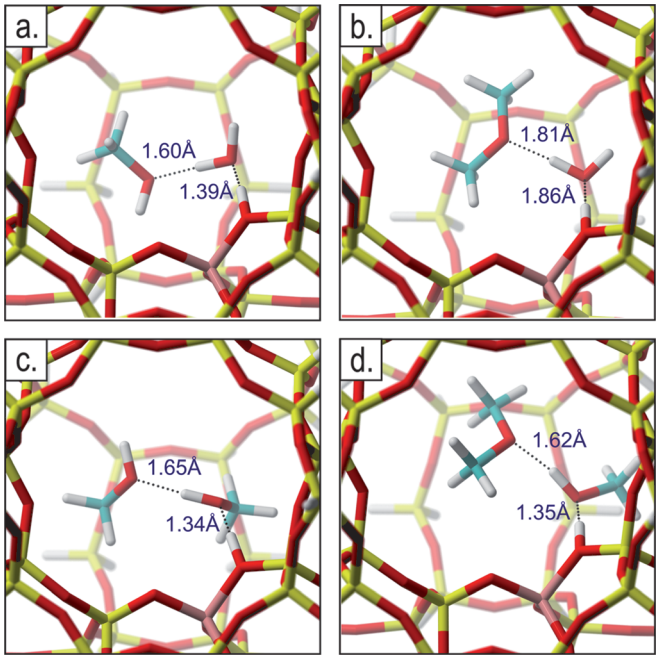

Figure 3. Co-adsorption of a,c) methanol or b,d) dimethyl ether on a previously adsorbed a,b) water or c,d) methanol molecule. Color code: Si, yellow; Al, pink; O, red; H, white; C, light blue.

or dimethyl ether on methanol, resulting in positive total adsorption free energies. However, in view of the very large entropic contributions, the static approach may no longer be sufficient, such that no definitive conclusions on the occurrence of such complexes should be drawn at this point.

Molecular dynamics

The co-adsorption behavior of water, methanol and dimethyl ether was further explored by means of MD simulations. A complete overview of all MD runs and the salient results is given in Table S1 (Supporting Information). The first simulation starts with water adsorbed at the acid site and a methanol molecule present in its vicinity. The different stages observed along the trajectory are shown in Figure 4 a–c. Methanol initially forms a hydrogen bond with the adsorbed water molecule, until after approximately 2.8 ps, methanol displaces the water to adsorb directly at the Brønsted acid site. The water molecule remains loosely bonded to methanol for approximately 4.4 ps, and then detaches to diffuse freely through the zeolite channel (its trajectory is illustrated in Figure 4 d). To confirm this result, the simulation was repeated, starting from a slightly different configuration, yielding essentially the same behavior. Similarly, two MD simulations in which a dimethyl ether molecule is placed nearby a water molecule adsorbed at the acid site result in dimethyl ether replacing water at the acid site. These simulations are in line with the static calculations predicting that methanol and dimethyl ether adsorb more strongly to the acid site than water. These results also agree with co-adsorption experiments performed by Ison and

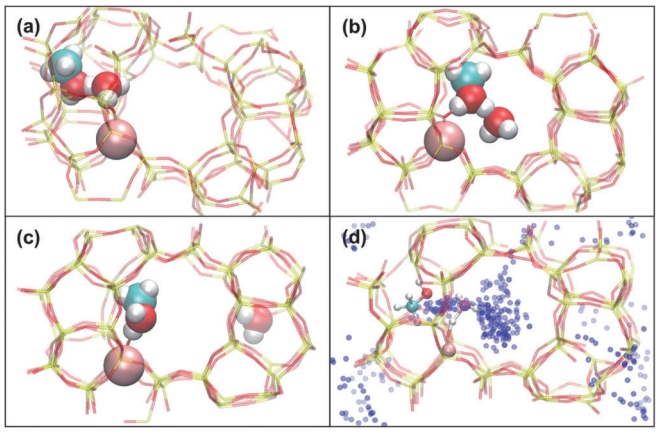

Figure 4. The three stages in the MD simulation of methanol and water in H-ZSM-5. a) Methanol initially bound to water, which in turn is bound to the acid site. b) Water bound to methanol, which is bound to the acid site. c,d) Methanol bound to the acid site, water floating freely through the zeolite channels. Color code: Si, yellow; Al, pink; O, red; H, white; C, light blue. The small blue spheres in (d) represent the path followed by the O_{MeOH} atom during the simulation. The Al defect is shown as a pink van der Waals sphere.

Gorte,[39] which also showed that water adsorbed onto the acid sites is rapidly displaced by methanol vapor.

Finally, two simulations were performed with a methanol and dimethyl ether molecule present in the neighborhood of the acid site. The first simulation starts from dimethyl ether adsorbed at the acid site, with methanol placed in the vicinity. Throughout the simulation, dimethyl ether remains bonded to the acid site and methanol freely floats through the channels (Figure 5 a,b). The second simulation starts with dimethyl ether

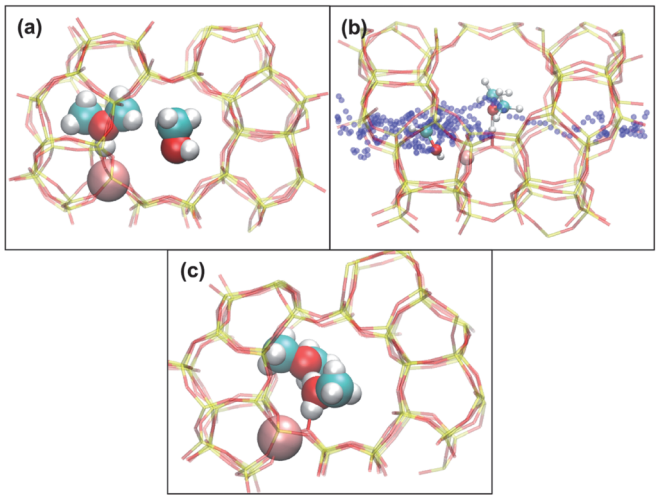

Figure 5. Different binding modes of methanol and dimethyl ether at the acid site. a,b) Dimethyl ether bound to the acid site, methanol floating freely through the channels. c) Dimethyl ether bound to methanol, which in turn is bound to the acid site. Color code: Si, yellow; Al, pink; O, red; H, white; C, light blue.

hydrogen-bonded to methanol, which is in turn bonded to the acid site (Figure 5 c). In contrast to water, methanol is not displaced but stays hydrogen-bonded to both the acid site and dimethyl ether. Both observed binding modes remain stable during a 25 ps simulation.

To estimate the barrier for replacing methanol by dimethyl ether, a metadynamics simulation was performed with two collective variables (CVs). The first CV represents the O–H bond breaking/forming between the dimethyl ether O atom and one of two H atoms. The second CV corresponds to the two O–H bonds between the methanol O atom and the same two H atoms. To account for bonds with different H atoms, bond lengths are represented by coordination numbers. Detailed information of the metadynamics simulation including a schematic representation of the CVs (Figure S1) can be found in the Supporting Information. The metadynamics simulation starts with methanol adsorbed at the acid site. The added Gaussian hills are combined to construct a 2D free energy surface, on which three stable states are visible (Figure 6). States (1) and (2) correspond to methanol adsorbed at the acid site with (1) dimethyl ether hydrogen-bonded to methanol and (2) dimethyl ether moving freely in the zeolite channels. State (4) corresponds to dimethyl ether adsorbed at the acid site with methanol moving freely. Interconversion between state (1, 2)

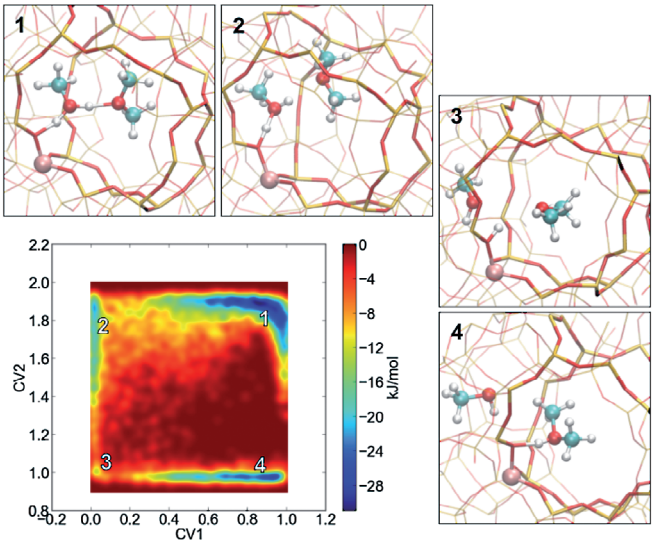

Figure 6. Free-energy surface of the competitive adsorption of methanol and dimethyl ether from a metadynamics simulation with two collective variables: CV1 = $CN(O_{DME}–H_{1,2})$, CV2 = $CN(O_{MeOH}–H_{1,2})$. Also shown are representative snapshots of the four (meta)stable states encountered along the trajectory. Color code in snapshots 1–4: Si, yellow; Al, pink; O, red; H, white; C, light blue.

on the one hand and state (4) on the other hand occurs through a metastable state (3) in which the acid site is unoccupied and both dimethyl ether and methanol are moving freely. States (1) and (4) are separated by a non-negligible barrier (≈27 kJ mol^{-1}), confirming the stability of both binding modes.

In summary, the MD and metadynamics simulations confirm the results from the static calculations, and provide more in-depth insights into the lifetime of the various complexes. At typical operating temperatures, dimethyl ether and methanol bind strongly to the acid site, and remain hydrogen-bonded to the acid site even if additional water or methanol molecules are present. The adsorption of water at the acid site is substantially weaker and it is rapidly replaced by methanol or dimethyl ether if either of these is present. Complexes in which methanol or dimethyl ether co-adsorb onto a water molecule hydrogen-bonded to the acid site are, therefore, unlikely to form or will quickly evolve toward more stable states. In contrast, methanol can remain hydrogen-bonded to the acid site in the presence of dimethyl ether, and a co-adsorption complex can be formed that remains stable during a fairly long MD run. The formation of co-adsorption complexes is thus plausible, and these can serve as the starting point for methoxide formation, as discussed below.

Methoxide formation

In the actual reaction step, the reactant complexes are reorganized to form a framework methoxide species from methanol or dimethyl ether, thereby releasing a water molecule or methanol molecule, respectively (see Scheme 1). Methoxide species are most likely to form on the framework oxygen atoms closest to the substitutional Al atom. With the Al locat-

ed in the T12 position, three of its adjacent oxygen atoms (O20, O24, and O11) are accessible from the channel system (see Figure 1). In static calculations, a specific framework oxygen is a priori selected as the recipient of the methyl group. We have opted to study the formation of methoxides on O24, such that transition states for the subsequent methylation reactions of different alkenes are similar in orientation to those encountered in the concerted methylation pathways from methanol and dimethyl ether (see below). In the metadynamics simulations, this limitation disappears automatically because coordination numbers are used as the collective variables, allowing a more general definition of a product state that includes methoxides on any of the three oxygens.

Table 2. Methoxide formation from methanol and dimethyl ether.[a]

	$\Delta H^{\ddagger}_{m}$ [kJ mol^{-1}]	$\Delta S^{\ddagger}_{m}$ [J mol^{-1} K^{-1}]	$-T\Delta S_{m}$ [kJ mol^{-1}]	$\Delta G^{\ddagger}_{m}$ [kJ mol^{-1}]	ΔH_{R} [kJ mol^{-1}]	ΔS_{R} [J mol^{-1}K^{-1}]	$-T\Delta S_{R}$ [kJ mol^{-1}]	ΔG_{R} [kJ mol^{-1}]
Methanol								
unassisted	132	4	−2	129	33	32	−20	13
methanol-assisted	136	−29	18	154	77	30	−18	59
Dimethyl ether								
unassisted	132	1	−1	131	54	41	−25	29
methanol-assisted	129	−28	17	146	83	27	−17	66

[a] Intrinsic enthalpy ($\Delta H^{\ddagger}_{m}$), entropy ($-T\Delta S^{\ddagger}_{m}$) and free energy ($\Delta G^{\ddagger}_{m}$) barriers; reaction enthalpy (ΔH_{R}), entropy ($-T\Delta S_{R}$) and free energy (ΔG_{R}) reported at 623 K. Level of theory electronic energy: ωB97X-D/6-31g(d,p)//ONIOM(B3LYP/6-31g(d,p):MNDO).

The results from the static calculations for methoxide formation with and without assisting methanol are summarized in Table 2. The table lists intrinsic enthalpy, entropy and free-energy barriers, reaction enthalpies, entropies, and free energies at 623 K. In the following, these results are systematically discussed alongside MD simulations using the metadynamics approach, which provide additional insights.

Unassisted methoxide formation

Methoxide formation occurs through a typical S_N2-type reaction, in which the methyl group undergoes an umbrella inversion upon transfer onto the framework. In the transition state (Figure 7a, b), the protonated methanol or dimethyl ether orients itself toward the center of the cavity, such that the breaking and forming C–O bonds are aligned, and the O–C–O atoms are almost perfectly collinear.

Intrinsic barriers for unassisted methoxide formation from methanol[1] and dimethyl ether are similar, both in terms of enthalpy ($\Delta H^{\ddagger} = 132$ kJ mol^{-1} for both methanol and dimethyl ether) and free energy ($\Delta G^{\ddagger} = 129$ kJ mol^{-1} for methanol; 131 kJ mol^{-1} for dimethyl ether). A similar barrier combined with a more favorable adsorption indicates that methoxide formation will be faster from dimethyl ether than from methanol. The reaction is endothermic in both cases, ($\Delta H_R = +33$ kJ mol^{-1} for methanol; $+54$ kJ mol^{-1} for dimethyl ether) but is entropically favorable because of the release of the water or methanol molecule, respectively, resulting in reaction free energies of $\Delta G_R = +13$ kJ mol^{-1} for methanol and $+29$ kJ mol^{-1} for dimethyl ether.

[1] *By following the intrinsic reaction coordinate (IRC) from the transition state to the reactant well for the reaction from methanol, a somewhat different methanol complex is obtained (see Figure S3), which is slightly higher in enthalpy ($\Delta H_{ads} = -98$ kJ mol^{-1}) and free energy ($\Delta G_{ads} = +2$ kJ mol^{-1}) than the most stable configuration shown in Figure 2. For consistency, reaction barriers are determined relative to the most stable configuration.*

In the early studies on small cluster models by Lesthaeghe et al.[24] and Vos et al.,[22] more distorted transition states were found, and much higher values were obtained for the reaction barriers, emphasizing the importance of the zeolite framework in stabilizing charged intermediates. Our results are generally in line with the findings of Maihom et al.[23] Although they used a different level of theory, the reactant, transition state and product geometries are very similar to those obtained here. For the barrier and reaction energies, only electronic energies at the ONIOM(M06-2X:UFF) level were reported, which are strictly speaking not directly comparable with the values included in Tables 1 and 2. A more detailed comparison is included in the Supporting Information.

The observation that methoxide formation from methanol or dimethyl ether is mechanistically analogous is also supported by the similar progress along the reaction coordinate reached in the transition states for both reactions, as inferred from the relative elongation of the breaking and forming

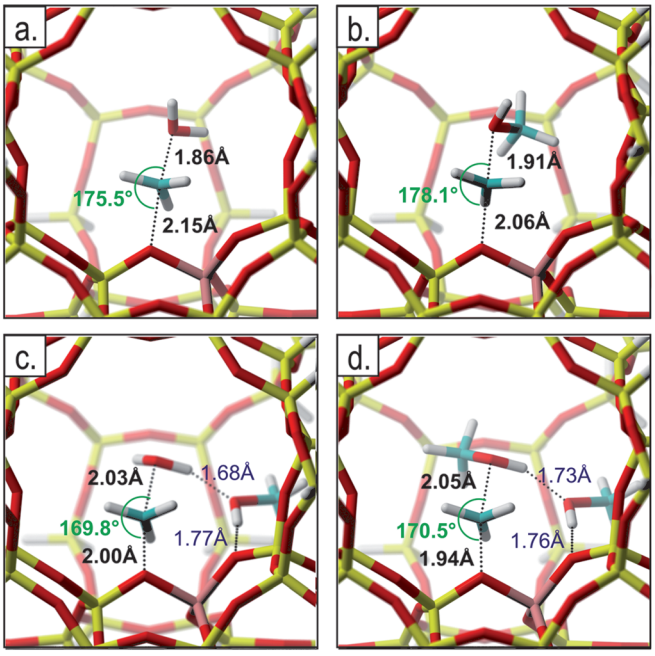

Figure 7. Transition states for a,b) unassisted and c,d) methanol-assisted methoxide formation from a,c) methanol and b,d) dimethyl ether.

bonds in the transition state compared to the reactant and product states, respectively.[40] These bond elongation percentages are listed in Table S3.

The methoxide formation was also studied using metadynamics simulations, which have proven to be a powerful tool for studying chemical reactions,[28] and, in particular, the effect of solvent molecules.[41,42] Two CVs are used: CV1 describes the breaking of the C–O bond by means of the coordination number between the methyl carbon and the oxygen of the reacting methanol or dimethyl ether molecule; CV2 tracks the C–O bond formation through the coordination number between the methyl carbon and the four framework oxygen atoms connected to aluminum. Additional details are given in the Supporting Information (Figure S2).

The resulting 2D free energy surfaces are shown in Figure 8. The sequence of events is very similar for methanol and dimethyl ether as the reactant, and corresponds fully with the S_N2-type reaction predicted by the static calculations. An approximate 1D profile is constructed from the 2D surface by taking the difference CV2−CV1 and projecting the 2D surface onto the diagonal running from the bottom right to the top left. In both cases, the 1D profile displays a broad transition state region. The red curves in the 1D plots display the changing probability of hydrogen bonding with the acid site along the trajectories. These results demonstrate that the breaking of the hydrogen bond between the dimethyl ether and the acid site occurs between values −0.6 and −0.2 on the 1D reaction coordinate, whereas for methanol this occurs much later, between −0.4 and −0.1. After the reactant is fully detached from the acid site, the free-energy profile becomes almost flat, indicating that the protonation of the reactant and subsequent formation of a separated ion pair is the rate-limiting phase in the reaction.

Although the reaction mechanisms are similar, the free-energy barrier for the forward reaction obtained from the metadynamics simulation (i.e., the difference between the transition state ensemble and the integrated free energy of the reactant region) is higher with methanol as the reactant (160 ± 5 kJ mol^{-1}) than with dimethyl ether (143 ± 2 kJ mol^{-1}). A possible explanation for this difference is the higher number of possible binding modes at the Brønsted site for methanol, resulting in a larger entropic penalty upon reaction. This conformational entropy cannot be accounted for in the static calculations, which are intrinsically restricted to a single point on the potential energy surface.

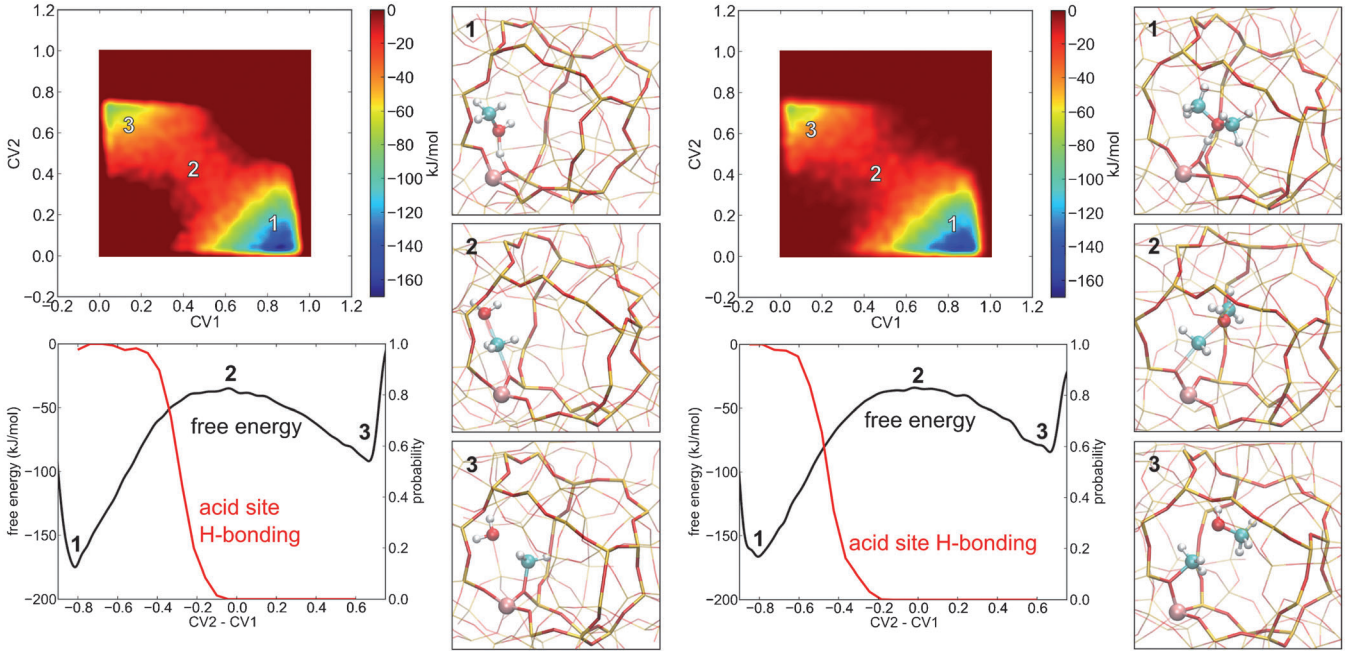

Figure 8. Free-energy surfaces of framework methoxide formation with methanol (left panel) and dimethyl ether (right panel) as the reactant, respectively, with CV1 = CN(C_X–O_X) and CV2 = CN(C_X–O_{zeo}), X = methanol or dimethyl ether. Representative snapshots illustrate the three phases of the reaction: (1) reactant basin, (2) transition state region, (3) product state. Color code: Si, yellow, Al, pink; O, red; H, white; C, light blue. Also shown are the free-energy profiles along a 1D reaction coordinate, respectively, taken as the difference between CV2 and CV1, and the probability of H-bonding with the acid site.

Methoxide formation assisted by methanol

Enthalpy ($\Delta H^{\neq}$), entropy ($-T\Delta S^{\neq}$), and free energy ($\Delta G^{\neq}$) barriers for the methanol-assisted methoxide formation are also included in Table 2. All results in this table are intrinsic values referred to the state in which both molecules are adsorbed close to the acid site. In the presence of an additional methanol molecule, the transition states are more ringlike, with additional hydrogen bonds formed in the transition state (see Figure 7c, d). In an ideal S_N2-reaction, the breaking and forming bonds are perfectly aligned; deviations from 180° are unfavorable and increase the barrier.[43] For the unassisted reactions, the O–C–O angle is quasi linear (175.5° for methanol and 178.1° for dimethyl ether). In the transition states with assisting metha-

nol, however, the O–C–O angle deviates slightly more from linearity, because the ringlike transition state needs to be formed; the O–C–O angle is reduced to 169.8° and 170.5° for methanol and dimethyl ether, respectively.

Interestingly, the participation of an additional methanol increases the free-energy barrier, for both methanol (from 129 to 154 kJ mol^{-1}) and dimethyl ether (from 131 to 146 kJ mol^{-1}). The effect on the enthalpy barrier is more subtle and does not show a clear trend; $\Delta H^{\neq}$ increases from 132 to 136 kJ mol^{-1} for methanol and decreases from 132 to 129 kJ mol^{-1} for dimethyl ether. Overall, these results indicate that the "assisting" methanol does not necessarily accelerate the reaction, in contrast to earlier reports based on small-cluster calculations. The additional electrostatic stabilization of assisting methanol on the transition states is largely outweighed by the effects of the zeolite lattice itself.

tant and transition states with indication of the hydrogen bond lengths and O–C–O angles is included in the Supporting Information (Figure S4). Assisted reactions are more endothermic compared with the unassisted methoxide formation. As a result, the transition states are delayed in the presence of assisting methanol, which is also reflected in the relative bond elongations (Table S3).

To obtain more insight into the process of methoxide formation at higher loadings, metadynamics simulations were also performed with five guest molecules in the unit cell. A first metadynamics simulation was performed with methanol as reactant in the presence of three additional methanol molecules and one molecule of water. The same CVs are used as in the simulation of the methoxide formation from a single methanol. The free-energy surface is shown in Figure 9 together with some representative snapshots of the different phases along

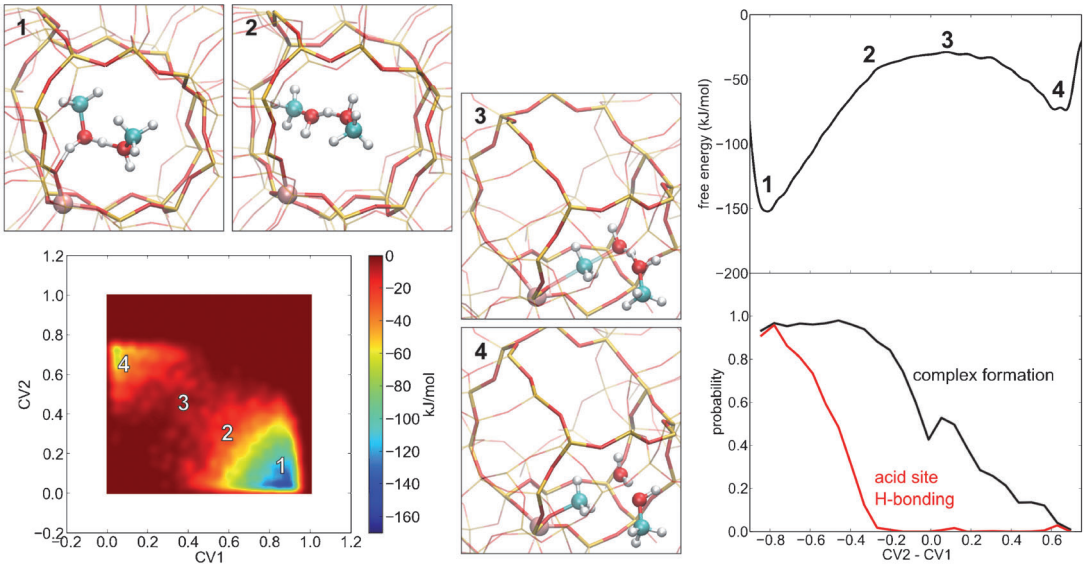

Figure 9. Left: Free-energy surface of framework methoxide formation with methanol in the presence of one water molecule and three additional methanol molecules. The four characteristic phases are indicated and illustrated with representative snapshots (color code: Si, yellow; Al, pink; O, red; H, white; C, light blue). For clarity, only molecules directly interacting with the reagents are shown. Top right: free energy along the 1D reaction coordinate, taken as the difference CV2−CV1. Bottom right: hydrogen bonding probability for methanol with a nearby methanol (black line) and with the acid site (red line) along the 1D reaction coordinate.

In the presence of an assisting methanol, the free-energy barriers contain a considerable entropic contribution ($-T\Delta S^{\neq} =$ 18 kJ mol^{-1} for methanol, 17 kJ mol^{-1} for dimethyl ether). The origin of this effect becomes clear when the geometrical features of the unassisted and assisted reactions are compared. For example, in the unassisted methoxide formation from methanol, the hydrogen bonds present in the reactant state (Figure 2a) disappear as the C–O bond with the framework starts to form in the transition state (Figure 7a), compensating the resulting entropy loss. In contrast, in the methanol-assisted reaction, both the reactant complex (Figure 3c) and the transition state (Figure 7c) are stabilized by hydrogen bonds, and the entropic penalty owing to the formation of the C–O bond is sustained. Similar effects are observed for methoxide formation from dimethyl ether. A side-by-side comparison of all reac-

the reaction pathway. The mechanism of methoxide formation reveals some distinct differences if additional protic molecules are present. The simulation starts with a methanol–methanol complex bound to the acid site as the most stable conformational state (phase 1). After proton transfer, the protonated complex detaches from the acid site, and stays mostly intact until approximately −0.2 on the 1D reaction coordinate, at which point a plateau is reached on the free-energy surface (phase 2). The clustering probability is very high and extends to well beyond the top of the barrier (phase 3), until the methoxide is formed and a free water molecule is produced (phase 4).

Compared with the unassisted reaction, the barrier height is lowered from 160 to 139 ± 2 kJ mol^{-1}. This finding is contrary to the static results (Table 2), which showed an increase of the

free-energy barrier in the methanol-assisted reaction from 129 to 154 kJ mol^{-1}, as a result of the formation of the entropically unfavorable ringlike transition state. In the metadynamics simulation, the proton transfer from the zeolite to the guest molecules and their separation from the acid site are almost completed before they are reoriented and the framework methoxide is formed. The reaction proceeds through a broader transition state region, mitigating the entropic penalty of the rigid transition structure obtained in the static calculations.

A second metadynamics simulation was performed with dimethyl ether as the reactant, accompanied by three methanol molecules and one water molecule. The simulation is started with dimethyl ether hydrogen-bonded to the acid site. The corresponding free-energy surface is shown in Figure 10. Similar to the reaction without assisting molecules, the system is activated by proton transfer from the acid site to dimethyl ether (phase 1). Subsequently, the protonated dimethyl ether is stabilized by hydrogen bonding with a nearby methanol molecule (phase 2). During the actual methyl transfer, the assisting molecule separates from the protonated dimethyl ether (phase 3) and the methoxide is formed (phase 4).

Unlike the reaction with methanol as the reactant, the presence of assisting molecules slightly increases the activation barrier from 143 to 149 $\pm$ 2 kJ mol^{-1}. This may be explained by the observation that for both the reaction from methanol and dimethyl ether the protonation and subsequent detaching from the framework (phase 1, 2) is the rate-limiting phase along the trajectory. In the case of dimethyl ether (Figure 10),

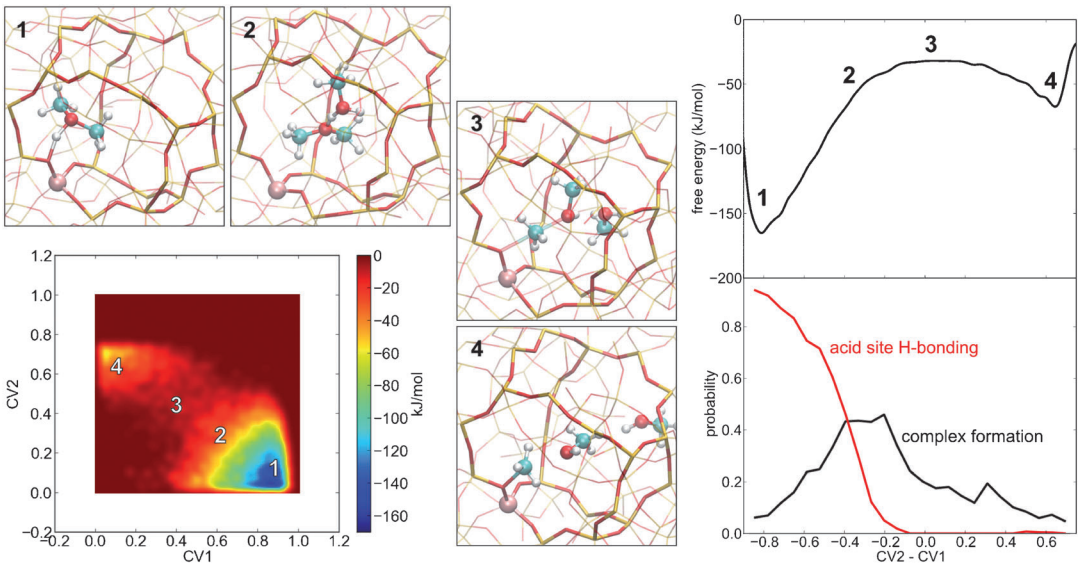

Figure 10. Left: Free-energy surface of framework methoxide formation with dimethyl ether in the presence of one water molecule and three additional methanol molecules. For details, see legend of Figure 9.

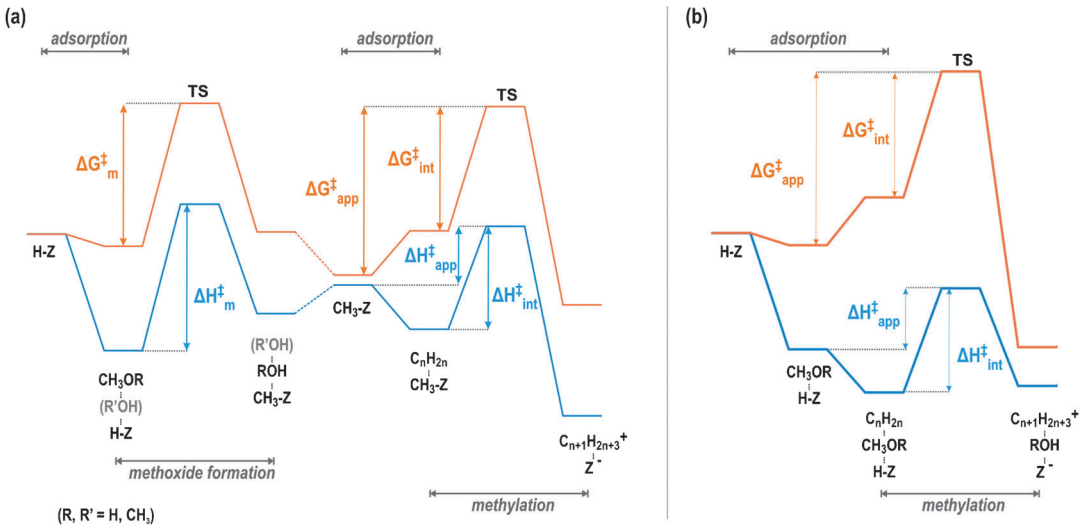

Figure 11. Schematic enthalpy (blue) and free-energy (orange) profiles for alkene methylation. a) Stepwise mechanism: after formation of a framework-bound methoxide (from methanol or dimethyl ether, with or without assisting molecules), the alkene co-adsorbs onto the methoxide and is subsequently methylated. b) Concerted mechanism: the alkene co-adsorbs onto a hydrogen-bonded methanol or dimethyl ether and is methylated in a single step.

an assisting methanol can only intervene once the proton transfer is completed and the protonated dimethyl ether is detached from the acid site, whereas in the reaction with methanol (Figure 9), additional methanol molecules can also assist in the proton-transfer phase. The effect of an additional methanol on the different phases along the trajectory can also be observed in the 1D profiles for the different simulations (Figure 8–10). Additional figures comparing the 1D profiles for the unassisted and assisted reactions from methanol and dimethyl ether are included in the Supporting Information (Figure S6).

Alkene methylation with methanol, dimethyl ether, and framework methoxides

Free-energy profiles and kinetic parameters are reported for the methylation of alkenes (ethene, propene, and *trans*-2-butene) with three methyl sources. Methylation with framework-bound methoxides (Figure 11 a) is compared with methylation with methanol or dimethyl ether in a concerted step (Figure 11 b). Scattered information on these reactions available in the literature is based on a variety of model systems and theoretical methods, encumbering the construction of an overall picture. Enthalpy ($\Delta H^{\ddagger}$), entropy ($-T\Delta S^{\ddagger}$) and free-energy barriers ($\Delta G^{\ddagger}$), as well as rate coefficients at 623 K (k) and Arrhenius parameters (E_a, A) for the methylation with methanol of ethene, propene, and *trans*-2-butene were reported in a recent paper by some of the authors.[44] Herein, methylation of these alkenes with dimethyl ether and framework-bound methoxides have been modeled using the same 46 T cluster model and levels of theory to allow mutual comparison between the three methyl sources. All results are listed side-by-side in Tables 3 and 4.

Apart from some subtle differences, the kinetics of all reactions are largely the same and thus one may conclude that the methoxide species are equally capable of performing methylation reactions once they are formed. The barrier for methoxide formation is somewhat higher than those for the actual methylation reactions, in line with previous reports.[22,23] Maihom et al. also studied ethene methylation with methanol, dimethyl ether, and framework-bound methoxides using an ONIOM approach.[23] Their reported energy barriers at the ONIOM(M06-2X:UFF) level of theory are again much higher than our current results (see also the discussion above regarding the methoxide

Table 3. Alkene methylation with framework methoxide, dimethyl ether, and methanol. Intrinsic enthalpy ($\Delta H^{\ddagger}$), entropy ($-T\Delta S^{\ddagger}$) and free-energy barriers ($\Delta G^{\ddagger}$); Unimolecular rate coefficients at 623 K (k) and Arrhenius parameters (E_a, A). Electronic energies are evaluated at ωB97X-D/6-31+G(d,p).

	CH_3–Z			H–Z + dimethyl ether			H–Z + CH_3OH[a]		
	$\Delta H^{\ddagger}_{int}$ [kJ mol^{-1}]	$-T\Delta S^{\ddagger}_{int}$ [kJ mol^{-1}]	$\Delta G^{\ddagger}_{int}$ [kJ mol^{-1}]	$\Delta H^{\ddagger}_{int}$ [kJ mol^{-1}]	$-T\Delta S^{\ddagger}_{int}$ [kJ mol^{-1}]	$\Delta G^{\ddagger}_{int}$ [kJ mol^{-1}]	$\Delta H^{\ddagger}_{int}$ [kJ mol^{-1}]	$-T\Delta S^{\ddagger}_{int}$ [kJ mol^{-1}]	$\Delta G^{\ddagger}_{int}$ [kJ mol^{-1}]
ethene	102	21	123	111	25	136	99	30	129
propene	93	19	112	94	24	118	94	21	114
trans-2-butene	84	24	108	90	23	112	92	21	113
	k_{int} [s^{-1}]	E_a [kJ mol^{-1}]	A [s^{-1}]	k_{int} [s^{-1}]	E_a [kJ mol^{-1}]	A [s^{-1}]	k_{int} [s^{-1}]	E_a [kJ mol^{-1}]	A [s^{-1}]
ethene	6.2E+02	107	5.7E+11	5.1E+01	116	2.6E+11	2.0E+02	104	1.0E+11
propene	5.3E+03	99	9.5E+11	1.8E+03	99	3.3E+11	3.3E+03	99	6.0E+11
trans-2-butene	1.1E+04	89	3.3E+11	5.0E+03	95	4.4E+11	4.1E+03	97	5.5E+11

[a] Previously reported in ref. [44].

Table 4. Alkene methylation with framework methoxide, dimethyl ether, and methanol. Apparent enthalpy ($\Delta H^{\ddagger}$), entropy ($-T\Delta S^{\ddagger}$) and free-energy barriers ($\Delta G^{\ddagger}$); Bimolecular rate coefficients at 623 K (k) and Arrhenius parameters (E_a, A). Electronic energies are evaluated at ωB97X-D/6-31+G(d,p).

	CH_3–Z			H–Z + dimethyl ether			H–Z + CH_3OH[a]		
	$\Delta H^{\ddagger}_{app}$ [kJ mol^{-1}]	$-T\Delta S^{\ddagger}_{app}$ [kJ mol^{-1}]	$\Delta G^{\ddagger}_{app}$ [kJ mol^{-1}]	$\Delta H^{\ddagger}_{app}$ [kJ mol^{-1}]	$-T\Delta S^{\ddagger}_{app}$ [kJ mol^{-1}]	$\Delta G^{\ddagger}_{app}$ [kJ mol^{-1}]	$\Delta H^{\ddagger}_{app}$ [kJ mol^{-1}]	$-T\Delta S^{\ddagger}_{app}$ [kJ mol^{-1}]	$\Delta G^{\ddagger}_{app}$ [kJ mol^{-1}]
ethene	77	81	158	76	97	172	82	78	160
propene	53	99	152	43	112	154	54	94	148
trans-2-butene	30	105	136	24	117	141	36	104	140
	k_{app} [m^3 mol^{-1} s^{-1}]	E_a [kJ mol^{-1}]	A [m^3 mol^{-1} s^{-1}]	k_{app} [m^3 mol^{-1} s^{-1}]	E_a [kJ mol^{-1}]	A [m^3 mol^{-1} s^{-1}]	k_{app} [m^3 mol^{-1} s^{-1}]	E_a [kJ mol^{-1}]	A [m^3 mol^{-1} s^{-1}]
ethene	4.0E−02	86	7.2E+05	2.3E−03	85	3.3E+04	2.7E−02	91	1.2E+06
propene	1.2E−01	63	2.2E+04	7.5E−02	52	1.8E+03	2.6E−01	64	5.8E+04
trans-2-butene	2.8E+00	40	6.2E+03	9.1E−01	34	6.0E+02	1.3E+00	45	8.4E+03

[a] Previously reported in ref. [44].

formation). A more detailed comparison of the numerical values is included in the Supporting Information (Table S4).

Conclusion

Herein, we have performed an in-depth study on the formation of methoxides from methanol or dimethyl ether, and their reactivity in alkene methylation reactions. In particular, the effect of additional water and methanol molecules present at typical operating conditions on the methoxide formation is investigated. Static DFT calculations on large cluster models are supplemented by ab initio molecular dynamics simulations to attain a more rigorous description of the dynamic properties of reactants and products, and account for the flexibility of the zeolite framework at operating temperatures.

These simulations have revealed that at higher temperatures both dimethyl ether and methanol adsorb strongly onto the zeolite acid site, whereas water forms a weaker adsorption complex. Consequently, water is quickly displaced by dimethyl ether or methanol, whereas methanol can stay hydrogen-bonded to the acid site in the presence of dimethyl ether. Stable co-adsorption complexes can be formed at the acid site in which dimethyl ether or a second methanol molecule adsorbs on top of the first methanol. Co-adsorption of the second molecule results in an increase of the adsorption enthalpy, but also causes an additional entropy loss. At typical reaction temperatures, the entropic penalty cancels out the enthalpic stabilization, resulting in positive total adsorption free energies. Molecular dynamics simulations have provided valuable additional insights into the kinetic and thermodynamic stability of the complexes considering the very large entropic contributions.

Methoxide formation from methanol or dimethyl ether was found to occur through similar mechanisms. Whereas earlier studies using small cluster models found that the presence of an assisting methanol stabilizes the transition state, decreasing the enthalpy barrier for methoxide formation, the effect is much less pronounced in our calculations using a large cluster model. Comparing unassisted and assisted methoxide formation, the enthalpy barrier changes only slightly, which indicates that the stabilizing effects of the zeolite framework largely outweigh the additional electrostatic stabilization of the assisting methanol. In the static calculations, ringlike transition states are obtained for the assisted reactions, resulting in an increased entropy loss and higher free-energy barriers.

Additional insights are obtained from metadynamics simulations. For the unassisted methoxide formation, the free-energy barrier derived from the metadynamics is higher for the reaction from methanol than from dimethyl ether, which may be owed to a better account of conformational entropy in the MD simulations. The metadynamics simulations also shed a different light on the effect of assisting methanol molecules, demonstrating that the proton transfer from the zeolite to the guest molecules is almost completed before reorientation and the actual formation of a framework methoxide, mitigating the entropic penalty of the ringlike transition structure obtained in the static calculations. For the reaction from methanol, this results in a lower free-energy barrier than for the unassisted reaction, whereas for dimethyl ether the participation of an additional methanol does not have a significant effect. Overall, the simulations performed in this study show that the formation of methoxide species is governed by many different factors and will ultimately depend on the precise reaction conditions. Methoxide formation from methanol may be accelerated by the presence of additional methanol molecules, whereas the reaction from dimethyl ether does not benefit greatly from methanol assistance.

Finally, we have compared the methylation of alkenes with methanol, dimethyl ether, and methoxide species, using the same computational scheme to obtain a systematic overview. This side-by-side comparison reveals that apart from some subtle differences the kinetics of all reactions are very similar. Importantly, comparison of the concerted methylation steps starting from methanol or dimethyl ether to methylation with framework-bound methoxide species confirms that the latter are equally reactive toward methylation once they are formed.

Experimental Section

Static calculations

A detailed description of the methodology has been given in previous work;[7,9,44] the key points are summarized below. Geometry optimizations were performed by using the two-level ONIOM-(B3LYP/6-31+G(d,p):MNDO) method, treating a central cluster of 8 T atoms and the guest molecules at the higher level of theory. Saturating hydrogen atoms are constrained in space to avoid unrealistic distortions of the zeolite model. Stationary points are characterized as minima or transition states by frequency calculations. Reactant and product complexes are localized by applying slight perturbations of the transition state along the imaginary frequency followed by full-geometry optimizations (quasi-IRC approach). Single-point calculations at the ωB97X-D/6-31+G(d,p) level of theory are performed to refine the energies of the various stationary points. The hybrid ωB97X-D functional includes both long-range corrections and dispersion interactions.[7,9,44] All geometry optimizations and energy refinements are performed with the Gaussian 03 and Gaussian 09 packages.[45–46] Initial geometries were constructed with ZEOBUILDER.[47–48] Partition functions are calculated from a normal mode analysis using a partial Hessian to exclude the terminating hydrogen atoms with constrained positions (PHVA approach). Enthalpy, entropy, and total free-energy profiles at 350 °C were calculated by using statistical thermodynamics. Rate constants in the temperature range 250–400 °C were determined from conventional transition-state theory. Arrhenius parameters were obtained from a standard fitting procedure. Normal mode analysis and all thermochemistry and chemical kinetics calculations were performed with the TAMKIN toolkit.[48–49]

Molecular dynamics

MD simulations were performed with the CP2K simulation package (version 2.4).[50] The dynamics of the nuclei was governed by the Newtonian equations of motion in which the potential from the Born–Oppenheimer electronic ground state is inserted. The self-consistent field energy was evaluated with DFT using the revPBE functional[51] with the DZVP–GTH basis set[52] and Grimme D3 dispersion corrections.[53] The integration time step was set to 0.5 fs.

After inserting the guest molecules inside the zeolite channels, the system was equilibrated for 5 ps, followed by a production run at 670 K and 1 bar in the isobaric-isothermal (NPT) ensemble. The canonical sampling with velocity rescaling algorithm was used for both the thermostat and the barostat.[54] An overview of the performed MD simulations is given in Table S1.

Metadynamics

Metadynamics simulations were performed in the canonical (NVT) ensemble at 670 K, by using cell parameters ($a=20.3528$ Å, $b=20.2144$ Å, $c=13.6141$ Å, and $\alpha=\beta=\gamma=90^\circ$) taken from the previously equilibrated NPT runs.[25] Gaussian hills were added every 25 fs to the 2D potential energy surface along two CVs. Although in principle any explicit function of the coordinates of the system can be used as CV, coordination numbers (CN) are ideally suited to describe the formation and breaking of chemical bonds. A CN between two sets of atoms i and j is defined as:

$$CN = \sum_{i,j} \frac{1-(r_{ij}/r_0)^{nn}}{1-(r_{ij}/r_0)^{nd}} \quad (1)$$

in which r_{ij} is the distance between atoms i and j. The parameters nn and nd were set to 6 and 12, respectively. The reference distance, r_0, was chosen to be near the transition state distance between atoms i and j. Note that this choice differs from the r_0 values chosen in our previous paper,[25] which produces a value for each CN term close to one at the bonding distance, approximately 0.5 at the transition state, and exponentially decaying at larger distances. In addition to the Gaussian hills, quadratic walls were added to restrict the simulations to an area of interest on the free-energy surface. An overview of the metadynamics simulations and CVs is given in Table S2. Additional details on the CVs used in specific simulations are included in the main text and/or in the Supporting Information.

The free-energy profile of the reaction was reconstructed from a metadynamics run based on the sum of the spawned Gaussian hills. The free energies were calculated as the mean free energy over the part of the simulation in which the barrier height starts to fluctuate and the dynamics along the reaction coordinate become diffusive. The statistical errors are computed as the standard deviation of the mean, after removal of correlated data values.[27] The resulting 2D free-energy surface was projected onto a 1D surface, taking the difference (CV2−CV1) as the reaction coordinate. From this 1D profile, the free-energy barrier ($\Delta G^{\ddagger}$) was calculated as the difference between the transition state ensemble and the integrated free energy of the reactant region.[25] The metadynamics simulations were continued until a statistical error of <5 kJ mol^{-1} on the barrier height is reached.

Acknowledgements

This work was supported by the Research Foundation Flanders (FWO), the Research Board of Ghent University (BOF), and BELSPO in the frame of IAP 7/05. Funding was also received from the European Research Council under the European Community's Seventh Framework Programme [FP7(2007-2013) ERC grant agreement number 240483]. Computational resources and services used in this work were provided by Ghent University (Stevin Supercomputer Infrastructure).

Keywords: kinetics · methylation · molecular dynamics · molecular modeling · zeolites

[1] M. Guisnet, J. P. Gilson, *Zeolites for Cleaner Technologies*, Imperial College Press, London, **2002**.
[2] U. Olsbye, S. Svelle, M. Bjørgen, P. Beato, T. V. W. Janssens, F. Joensen, S. Bordiga, K. P. Lillerud, *Angew. Chem. Int. Ed.* **2012**, *51*, 5810 – 5831; *Angew. Chem.* **2012**, *124*, 5910 – 5933.
[3] K. Hemelsoet, J. Van der Mynsbrugge, K. De Wispelaere, M. Waroquier, V. Van Speybroeck, *ChemPhysChem* **2013**, *14*, 1526 – 1545.
[4] S. Svelle, P. O. Rønning, S. Kolboe, *J. Catal.* **2004**, *224*, 115 – 123.
[5] S. Svelle, P. Ronning, U. Olsbye, S. Kolboe, P. O. Rønning, *J. Catal.* **2005**, *234*, 385 – 400.
[6] S. Saepurahman, M. Visur, U. Olsbye, M. Bjørgen, S. Svelle, *Top. Catal.* **2011**, *54*, 1293 – 1301.
[7] J. Van der Mynsbrugge, M. Visur, U. Olsbye, P. Beato, M. Bjørgen, V. Van Speybroeck, S. Svelle, *J. Catal.* **2012**, *292*, 201 – 212.
[8] S. Svelle, C. Tuma, X. Rozanska, T. Kerber, J. Sauer, *J. Am. Chem. Soc.* **2009**, *131*, 816 – 825.
[9] V. Van Speybroeck, J. Van der Mynsbrugge, M. Vandichel, K. Hemelsoet, D. Lesthaeghe, A. Ghysels, G. B. Marin, M. Waroquier, *J. Am. Chem. Soc.* **2011**, *133*, 888 – 899.
[10] I. M. Hill, S. A. Hashimi, A. Bhan, *J. Catal.* **2012**, *285*, 115 – 123.
[11] I. M. Hill, S. A. Hashimi, A. Bhan, *J. Catal.* **2012**, *291*, 155 – 157.
[12] S. Svelle, M. Visur, U. Olsbye, M. Bjørgen, *Top. Catal.* **2011**, *54*, 897 – 906.
[13] T. R. Forester, S.-T. Wong, R. F. Howe, *J. Chem. Soc. Chem. Commun.* **1986**, 1611 – 1613.
[14] T. R. Forester, R. F. Howe, *J. Am. Chem. Soc.* **1987**, *109*, 5076 – 5082.
[15] P. Cheung, A. Bhan, G. J. Sunley, D. J. Law, E. Iglesia, *J. Catal.* **2007**, *245*, 110 – 123.
[16] I. Ivanova, A. Corma, *J. Phys. Chem. B* **1997**, *101*, 547 – 551.
[17] W. Wang, A. Buchholz, M. Seiler, M. Hunger, *J. Am. Chem. Soc.* **2003**, *125*, 15260 – 15267.
[18] Y. Jiang, M. Hunger, W. Wang, *J. Am. Chem. Soc.* **2006**, *128*, 11679 – 11692.
[19] W. Wang, M. Hunger, *Acc. Chem. Res.* **2008**, *41*, 895 – 904.
[20] Y. Ono, T. Mori, *J. Chem. Soc. Faraday Trans. 1* **1981**, *77*, 2209 – 2221.
[21] J. Rakoczy, T. Romotowski, *Zeolites* **1993**, *13*, 256 – 260.
[22] A. M. Vos, K. H. L. Nulens, F. De Proft, R. A. Schoonheydt, P. Geerlings, *J. Phys. Chem. B* **2002**, *106*, 2026 – 2034.
[23] T. Maihom, B. Boekfa, J. Sirijaraensre, T. Nanok, M. Probst, J. Limtrakul, *J. Phys. Chem. C* **2009**, *113*, 6654 – 6662.
[24] D. Lesthaeghe, V. Van Speybroeck, G. B. Marin, M. Waroquier, *Angew. Chem. Int. Ed.* **2006**, *45*, 1714 – 1719; *Angew. Chem.* **2006**, *118*, 1746 – 1751.
[25] S. L. C. Moors, K. De Wispelaere, J. Van der Mynsbrugge, M. Waroquier, V. Van Speybroeck, *ACS Catal.* **2013**, *3*, 2556 – 2567.
[26] G. Bussi, A. Laio, M. Parrinello, *Phys. Rev. Lett.* **2006**, *96*, 090601.
[27] A. Laio, F. L. Gervasio, *Rep. Prog. Phys.* **2008**, *71*, 126601 – 126601.
[28] A. Laio, M. Parrinello, *Proc. Natl. Acad. Sci. USA* **2002**, *99*, 12562 – 12566.
[29] J. Dědeček, D. Kaucký, B. Wichterlová, *Chem. Commun.* **2001**, 970 – 971.
[30] S. Sklenak, J. Dedeček, C. Li, B. Wichterlová, V. Gábová, M. Sierka, J. Sauer, *Phys. Chem. Chem. Phys.* **2009**, *11*, 1237 – 1247.
[31] S. Sklenak, J. Dedecek, C. Li, B. Wichterlová, V. Gábová, M. Sierka, J. Sauer, *Angew. Chem. Int. Ed.* **2007**, *46*, 7286 – 7289; *Angew. Chem.* **2007**, *119*, 7424 – 7427.
[32] C. C. Lee, R. J. Gorte, W. E. Farneth, *J. Phys. Chem. B* **1997**, *101*, 3811 – 3817.
[33] J. Van der Mynsbrugge, K. Hemelsoet, M. Vandichel, M. Waroquier, V. Van Speybroeck, *J. Phys. Chem. C* **2012**, *116*, 5499 – 5508.
[34] I. C. Arik, J. F. Denayer, G. V. Baron, *Microporous Mesoporous Mater.* **2003**, *60*, 111 – 124.
[35] J. F. M. Denayer, W. Souverijns, P. A. Jacobs, J. A. Martens, G. V. Baron, S. Al, *J. Phys. Chem. B* **1998**, *102*, 4588 – 4597.
[36] B. A. De Moor, M.-F. Reyniers, O. C. Gobin, J. A. Lercher, G. B. Marin, *J. Phys. Chem. C* **2011**, *115*, 1204 – 1219.
[37] B. A. De Moor, M.-F. Reyniers, G. B. Marin, *Phys. Chem. Chem. Phys.* **2009**, *11*, 2939 – 2958.

[38] C. M. Nguyen, M.-F. Reyniers, G. B. Marin, *Phys. Chem. Chem. Phys.* **2010**, *12*, 9481 – 9493.
[39] A. Ison, R. J. Gorte, *J. Catal.* **1984**, *89*, 150 – 158.
[40] V. Van Speybroeck, Y. Martelé, M. Waroquier, E. Schacht, *J. Am. Chem. Soc.* **2001**, *123*, 10650 – 10657.
[41] A. Pavlova, E. J. Meijer, *ChemPhysChem* **2012**, *13*, 3492 – 3496.
[42] G. A. Gallet, F. Pietrucci, W. Andreoni, *J. Chem. Theory Comput.* **2012**, *8*, 4029 – 4039.
[43] D. Lesthaeghe, V. Van Speybroeck, G. B. Marin, M. Waroquier, *J. Phys. Chem. B* **2005**, *109*, 7952 – 7960.
[44] J. Van der Mynsbrugge, J. De Ridder, K. Hemelsoet, M. Waroquier, V. Van Speybroeck, *Chem. Eur. J.* **2013**, *19*, 11568 – 11576.
[45] Gaussian 03, Revision E.01, M. J. Frisch et al.—see Supporting Information.
[46] Gaussian 09 (Revision B.01): M. J. Frisch et al.—see Supporting Information.
[47] T. Verstraelen, V. Van Speybroeck, M. Waroquier, *J. Chem. Inf. Model.* **2008**, *48*, 1530 – 1541.
[48] *CMM Software*, molmod.ugent.be/software/.
[49] A. Ghysels, T. Verstraelen, K. Hemelsoet, V. Van Speybroeck, M. Waroquier, *J. Chem. Inf. Model.* **2010**, *50*, 1736 – 1750.
[50] J. VandeVondele, M. Krack, F. Mohamed, M. Parrinello, T. Chassaing, J. R. Hutter, *Comput. Phys. Commun.* **2005**, *167*, 103 – 128.
[51] K. Yang, J. J. Zheng, Y. Zhao, D. G. Truhlar, *J. Chem. Phys.* **2010**, *132*, 10.
[52] S. Goedecker, M. Teter, J. Hutter, *Phys. Rev. B* **1996**, *54*, 1703 – 1710.
[53] S. Grimme, J. Antony, S. Ehrlich, H. Krieg, *J. Chem. Phys.* **2010**, *132*, 154104 – 154104.
[54] G. Bussi, D. Donadio, M. Parrinello, *J. Chem. Phys.* **2007**, *126*, 014101.

Received: March 19, 2014
Published online on ■■ ■■, 0000

*J. Van der Mynsbrugge, S. L. C. Moors, K. De Wispelaere, V. Van Speybroeck**

■■ – ■■

Insight into the Formation and Reactivity of Framework-Bound Methoxide Species in H-ZSM-5 from Static and Dynamic Molecular Simulations

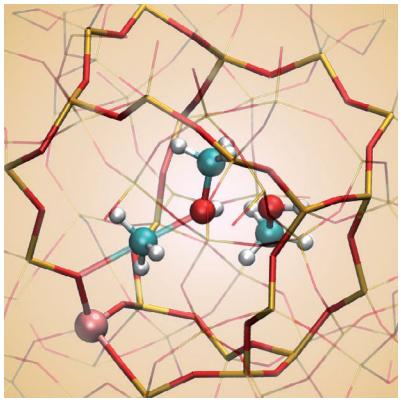

How may I assist you? The formation of framework-bound methoxides from methanol or dimethyl ether in zeolite H-ZSM-5 is investigated by a combination of static and dynamic simulations. Additional methanol molecules assist the proton transfer, which is the rate-limiting phase, in the methoxide formation from methanol, but not from dimethyl ether.